A CSI Feedback Framework based on Transmitting the Important Values and Generating the Others

Zhilin Du, Zhenyu Liu, *Member, IEEE*, Haozhen Li, *Graduate Student Member, IEEE*, Shilong Fan, Xinyu Gu, *Member, IEEE*, and Lin Zhang, *Member, IEEE*

***Abstract*—The application of deep learning (DL)-based channel state information (CSI) feedback frameworks in massive multiple-input multiple-output (MIMO) systems has significantly improved reconstruction accuracy. However, the limited generalization of widely adopted autoencoder-based networks for CSI feedback challenges consistent performance under dynamic wireless channel conditions and varying communication overhead constraints. To enhance the robustness of DL-based CSI feedback across diverse channel scenarios, we propose a novel framework, ITUG, where the user equipment (UE) transmits only a selected portion of critical values in the CSI matrix, while a generative model deployed at the BS reconstructs the remaining values. Specifically, we introduce a scoring algorithm to identify important values based on amplitude and contrast, an encoding algorithm to convert these values into a bit stream for transmission using adaptive bit length and a modified Huffman codebook, and a Transformer-based generative network named TPMVNet to recover the untransmitted values based on the received important values. Experimental results demonstrate that the ITUG framework, equipped with a single TPMVNet, achieves superior reconstruction performance compared to several high-performance autoencoder models across various channel conditions.**

***Index Terms*—Massive MIMO, Transformer model, CSI feedback, masked Autoencoder**

I. Introduction

Massive multiple-input multiple-output (MIMO) technology enhances spectrum and energy efficiency in wireless systems by enabling accurate downlink channel state information (CSI) at the base station (BS) or gNodeB (gNB). In frequency-division duplexing (FDD) systems, this downlink CSI must be transmitted from the user equipment (UE) to the BS, resulting in substantial communication overhead. The already large frequency bandwidth and high number of antennas lead to a high-dimensional CSI matrix, which further intensifies this overhead. Consequently, compressing the CSI matrix while ensuring accurate reconstruction has become essential for efficient operation in FDD systems.

Compressive sensing (CS) methods have been applied to compress the CSI by leveraging intrinsic channel properties, such as sparsity in the spatial [1] or temporal [2] domains. However, the effectiveness of CS approaches depends on a strict sparsity condition, which may not always be satisfied. Consequently, recent research has increasingly focused on using deep neural networks (DNNs) for CSI feedback. Since the introduction of the first autoencoder-based model for this purpose [3], numerous high-performance network structures for CSI feedback have emerged [4]–[11], achieving significantly improved reconstruction accuracy.

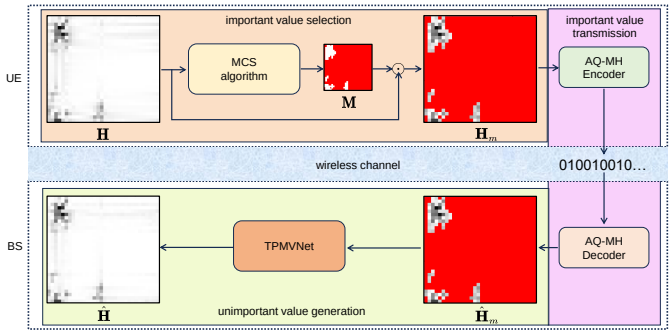

Fig. 1. Architecture of the proposed ITUG CSI feedback framework.

Although these autoencoder-based networks achieve promising results in CSI feedback, further studies on the practical deployment of DL-based CSI feedback reveal that autoencoder models are sensitive to data variations and have limited adaptability to natural data drift in wireless communications, where data distribution shifts over time [12]–[14]. The effectiveness of an autoencoder model relies heavily on the similarity between the training and deployment environments, meaning a model trained on CSI data from a specific channel environment may experience performance degradation when applied in a new environment [13], [14].

To improve the generalization capability of autoencoder networks in CSI feedback, ensuring they perform across a broader range of environments, various approaches have focused on training models with more diverse data that cover complex conditions. To capture data representing each local channel state of the participating UEs, frameworks like federated learning (FL) or similar distributed setups have been employed, enabling collaborative training of a global CSI model with input from both the BS and UEs [15]–[18]. While FL can produce models better suited to the participating UEs, it requires these UEs to meet demanding communication and memory requirements, which is often impractical for current mobile devices. Another approach leverages CSI generators

This work was supported in part by the National Natural Science Foundation of China (NSFC) under Grant 62201089, and in part by the National Key Research and Development Program under Grant 2022YFF0610303.

Z. Du, H. Li, S. Fan, X. Gu, L. Zhang are with the School of Artificial Intelligence, Beijing University of Posts and Telecommunications, Beijing, 100876, China (e-mail: {duzhilin, lihaozhen, fansl, guxinyu, zhanglin}@bupt.edu.cn). Zhenyu Liu is with the 5GIC and 6GIC, Institute for Communication Systems, University of Surrey, GU2 7XH Guildford, U.K. (e-mail: zhenyu.liu@surrey.ac.uk). X. Gu is also with the Future Network Center in Purple Mountain Laboratories, Nanjing 211111, China.

to represent local channel conditions, generating synthetic samples for data augmentation to enhance the training set. Techniques such as generative adversarial networks (GANs) [19], [20] and variational autoencoders (VAEs) [21] have been explored for this purpose; however, these generators require additional CSI data for training. Additional augmentation strategies include random delay adjustments [22], exploiting temporal or uplink correlations [23], or other specialized designs [24]. Approaches like multi-task learning [14], [25] and few-shot learning [26] have also been investigated, yet they raise concerns about generalization reliability, limiting their confidence for deployment across diverse conditions.

Many studies aim to enhance model performance by updating it when deployed in new scenarios where performance degradation is detected. For instance, [27] employs a few new data samples to fine-tune the model, while [28] introduces a continuous learning scheme to mitigate catastrophic forgetting during fine-tuning. In contrast, [29] proposes a model update strategy that requires no new data, using only the compressed codeword. Additionally, knowledge distillation (KD) approaches [30], [31] and meta-learning techniques [32], [33] enable the derivation of a local model from a shared global model with minimal training phases. However, these approaches require continuous performance monitoring during deployment and entail additional training phases, thereby consuming extra computational resources.

Given the intrinsic limitations of the autoencoder structure in generalization, some recent research has explored non-autoencoder approaches to tackle the CSI feedback problem. For instance, several studies have focused on codebook-based CSI feedback systems, where the UE transmits selected parts of a codebook, and a DNN at the BS refines this codebook vector to reconstruct the CSI information [34], [35]. Another line of research involves selectively discarding certain information at the UE, such as uniformly downsampling [36], [37], selecting only the high-magnitude values [38], or applying principal component analysis (PCA) [39]. However, these approaches often lack mechanisms for recovering the omitted information. A recent method [40], however, advances this idea by extracting key factors, such as delay and spread, from the CSI matrix, transmitting only these factors. Although this reduces the data to be transmitted, the processes of factor extraction and CSI matrix reconstruction still require a model, often using a Transformer-based network, to be completed.

To address the limited generalization ability of current autoencoder-based CSI feedback methods, we propose a novel and efficient CSI feedback framework. This framework operates by omitting certain CSI values at the UE side to reduce communication overhead, while introducing a refinement module at the BS to enhance reconstruction performance. By excluding neural networks or learnable parameters at the UE, the algorithm remains adaptable across diverse environments, free from adjustments specific to any single deployment scenario, thereby preserving its generalization ability. Specifically, our contributions are summarized as follows:

- We propose a CSI feedback framework named ITUG. Unlike traditional autoencoders, ITUG selects only a few important values from the CSI matrix for transmission, discarding the rest to reduce communication overhead. At the BS, a Transformer-based generative model reconstructs the masked, untransmitted values. The absence of deep learning components at the UE side enhances ITUG's adaptability across diverse environments, while the generative model at the BS ensures high reconstruction accuracy.
- We categorize the values in a CSI matrix into three groups—important values, unimportant values, and predictable values—based on their occurrence patterns and the physical characteristics of the wireless channel. To identify the high-scoring values as important values for transmission, we introduce a specific scoring method, named MCS, which evaluates each value based on its magnitude and contrast within the CSI matrix.
- We design an algorithm named AQ-MH to convert the important values into a bit sequence for transmission. AQ-MH encodes the values and their indices separately, using adaptive quantization bit lengths and a modified Huffman codebook, respectively. These methods work together to significantly reduce the bit count required for transmission while preserving transmission precision.
- We propose a Transformer-based generative network structure named TPMVNet, which is deployed on the BS side to recover the masked values that are not transmitted to the BS, using the important values as a reference. We design the data pre-processing, the forward propagation process based on the model structure, and the output post-processing methods. Additionally, we define the training and deployment schemes for TPMVNet.

II. System Model

A. Downlink CSI Preprocessing

We consider a single-cell MIMO FDD link, where a BS equipped with an N_t-antenna uniform linear array (ULA) serves multiple single-antenna UEs. In accordance with 3GPP technical specifications, sparse pilot symbols (CSI-RS) are distributed across the frequency domain for downlink transmission. Each subband contains N_f subcarriers, with a subcarrier spacing of Δf and a pilot spacing of ΔN subcarriers. Thus, adjacent pilots are separated by $\Delta N \cdot \Delta f$ Hz.

Let $\mathbf{h}_i \in \mathbb{C}^{N_p \times 1}$ represent the downlink CSI between the i-th antenna in the BS's ULA and the UE. Consequently, the pilot-sampled downlink CSI matrix $\tilde{\mathbf{H}}$, which captures the transmission links between all BS antennas and the UE, can be expressed as:

$$\tilde{\mathbf{H}} = \mathbf{H}_{all}\mathbf{Q}_{\Delta N} = [\mathbf{h}_1\ \mathbf{h}_2\ \cdots\ \mathbf{h}_{N_t}]^H \in \mathbb{C}^{N_t \times N_p}, \quad (1)$$

where $\mathbf{Q}_{\Delta N}$ is a downsampling matrix determined by the pilot rate ΔN, and $\mathbf{H}_{all}$ is the full downlink CSI matrix that contains the channel information of all subcarriers.

Next, the subcarrier-antenna domain CSI matrix $\tilde{\mathbf{H}}$ is transformed into the delay-angular domain to exploit its sparsity. This transformation is performed using a two-dimensional discrete Fourier transform (2D-DFT). The resulting transformed CSI matrix, $\mathbf{H}_{ad}$, is given by

$$\mathbf{H}_{ad} = \mathbf{F}_a^H \tilde{\mathbf{H}} \mathbf{F}_d, \tag{2}$$

where $\mathbf{F}_a$ and $\mathbf{F}_d$ are the $N_t \times N_t$ and $N_p \times N_p$ unitary DFT matrices, respectively. The UE then compresses and transmits a normalized version of the CSI matrix, denoted as $\mathbf{H}$, where the values of $\mathbf{H}_{ad}$ are scaled to the range of [-1, 1]. The BS receives the scaled CSI matrix $\hat{\mathbf{H}}$ and then recovers the subcarrier-antenna domain channel coefficients by applying the inverse discrete Fourier transform (IDFT).

B. CSI Compression and Reconstruction

To reduce communication overhead, the CSI matrix $\mathbf{H}$ undergoes compression before being transmitted through the wireless channel. After compression, the CSI matrix is quantized and encoded into a binary sequence $\mathbf{s}$. This sequence of operations at the UE can be expressed as

$$\mathbf{b} = f_{en}(\mathbf{H}; \theta_{en}), \tag{3}$$

where f_{en} represents the entire process of compression, quantization, and encoding. The term θ_{en} refers to the set of learnable parameters involved in the process, in cases where deep learning methods are utilized.

The binary sequence $\mathbf{b}$ is transmitted through the wireless channel and received by the BS as $\hat{\mathbf{b}}$. The BS then applies a series of algorithms to transform the sequence and reconstruct the CSI matrix $\hat{\mathbf{H}}$, maintaining the same dimensions as the original matrix $\mathbf{H}$. This reconstruction process can be expressed as

$$\hat{\mathbf{H}} = f_{de}(\hat{\mathbf{b}}; \theta_{de}), \tag{4}$$

where f_{de} represents the reconstruction operations, and θ_{de} denotes the set of learnable parameters, applicable if deep learning models are utilized in the process.

III. The Proposed ITUG Framework

The main concept of the ITUG framework is that the UE only transmits a small fraction of the important values in a CSI matrix. Meanwhile, a neural network in the BS is responsible for generating the large fraction of unimportant values that are not transmitted by the UE. As depicted in Fig. 1, the ITUG framework comprises three parts:

- **Important Value Selection:** Due to the limitation of communication overhead, the UE must select the most important values for effectively representing the CSI matrix. To address this, we propose an important value selection algorithm based on the magnitude and local contrast relative to nearby values. We refer to this algorithm as Magnitude and Contrast-based Selection, abbreviated as MCS. This algorithm is detailed described in Sec. IV.
- **Important Value Transmission:** The values and positions of the important values, represented by the sparse matrix $\mathbf{H}_m$ in Fig. 1, must be converted into a binary sequence for transmission. To optimize bit usage, we propose an adaptive bit length for quantizing the values into binary form and employ a modified Huffman encoding codebook, as described in [38], to encode the positions of the important values. The resulting binary sequences, which represent both the values and their positions, are transmitted to the BS via a wireless channel. At the BS, the values and positions of the important values are recovered to reconstruct $\hat{\mathbf{H}}_m$. We refer to this encoding and decoding process as Adaptive Quantization and Modified Huffman Encoding, abbreviated as AQ-MH. The whole process of encoding and decoding is discussed in Sec. V.
- **Unimportant Value Generation:** The unimportant values discarded by the UE during transmission are padded with zeros at the corresponding positions in $\hat{\mathbf{H}}_m$. At the BS, we design a Transformer-based model, called TPMVNet, to predict these masked unimportant values. The structure, training, and deployment of TPMVNet are described in detail in Sec. VI.

IV. Selecting the Important Values

The important values are those selected for transmission, as they need to effectively represent the channel and help the generative model, TPMVNet, at the BS predict the masked values that are not transmitted. Additionally, the number of important values needs to remain small to reduce communication overhead. The following sections identify the important values in the CSI matrix and use the MCS algorithm to select them.

A. Categorizing the Values in CSI Matrices

Through extensive observation of channel matrices, we found that the values in the channel matrix can be categorized into three types. The first type consists of values with large or small magnitudes that appear at irregular locations, which we refer to as important values. These values physically represent the angles or delay components associated with strong energy clusters in the propagation environment. The second type includes values that reside within the same delay or angular resolution as the important values and exhibit a clear gradual change in magnitude; we refer to these as predictable values. The third type consists of values that are contiguous and with magnitudes close to zero, referred to as unimportant values. These locations contain little to no channel energy.

In Fig. 2, we present three representative channel matrix samples, with the important values, predictable values, and unimportant values labeled accordingly. It can be observed that the important values, shown in the red boxes in Fig. 2, constitute only a small proportion of the total values in a channel matrix. Given that these values are crucial for defining the channel matrix and appear in irregular locations, we prioritize transmitting these values and ensure their accuracy in the reconstructed channel matrix. For the numerous unimportant values, we choose not to transmit them, as directly replacing them with zeros in the reconstructed CSI matrix has minimal impact.

For the predictable values, the reason we refer to them as "predictable" is that they represent the energy spread in the delay and angular domain, which is a common phenomenon in wireless channels. This means that as long as the matrix is a channel matrix, and the strong energy clusters are given,

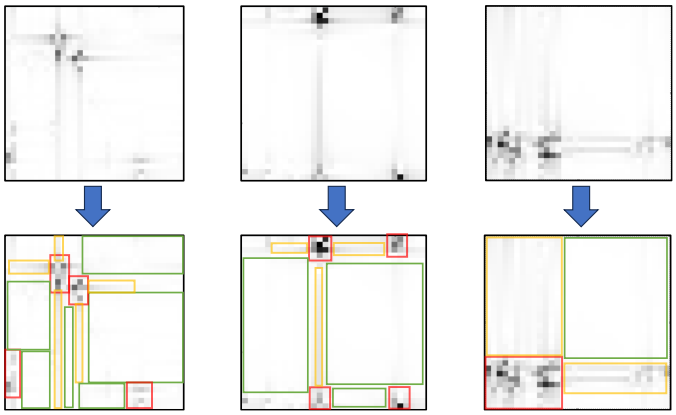

Fig. 2. Illustration of channel matrix value classification: red boxes represent important values, yellow boxes represent predictable values, and green boxes represent unimportant values.

the surrounding energy spread can be predicted. Consequently, these predictable values are also not transmitted because the TPMVNet at the BS is expected to learn the occurrence patterns of the predictable values in all channel matrices and exhibit the ability to generate them based on the input of the important values.

B. The MCS Algorithm for Selecting Important Values

According to the definition of important values in Sec. IV-A, an important value exhibits two main characteristics: it has a large (or sometimes small) amplitude and appears without any regularity or pattern. Based on these two characteristics, we develop a unified algorithm MCS to assign a score to each value in the CSI matrix. The higher the score, the more prominently these characteristics are exhibited, increasing the likelihood that the values will be considered as important values. For a value at the i-th row and j-th column in the CSI matrix, its score, $score_{i,j}$, is calculated based on two components. The first component is the amplitude of the value, $a_{i,j}$, representing the first characteristic for identifying important values. The second component is the average of the differences between the amplitude of the value and those of its neighboring values, reflecting the second characteristic. The calculating method is detailed as

$$score_{i,j} = a_{i,j} + d(i,j), \tag{5}$$

$$d(i,j) = \frac{1}{4}(|a_{i,j} - a_{i,j-1}| + |a_{i,j} - a_{i,j+1}| + |a_{i,j} - a_{i-1,j}| + |a_{i,j} - a_{i+1,j}|), \tag{6}$$

$$a_{i,j} = \sqrt{real(\mathbf{h}_{i,j})^2 + imag(\mathbf{h}_{i,j})^2}, \tag{7}$$

where $\mathbf{h}_{i,j}$ is the element of $\mathbf{H}$ at the i-th row and the j-th column.

Then, the important values are selected from the one with the highest score to the next until the sum of the score of the selected values reaches a threshold. The threshold, marked as θ_{UE}, is a proportion of the summed score of all elements in $\mathbf{H}$. The indices of the important values are marked in $\mathbf{M}$, as shown in Fig. 1, where "1" indicates the positions of important values, and "0" represents the positions that are masked and discarded during transmission. The masked CSI matrix to be transmitted, $\mathbf{H}_m$, is then obtained by

$$\mathbf{H}_m = \mathbf{H} \odot \mathbf{M}, \tag{8}$$

where $\odot$ denotes the Hadamard product or element-wise product. The complete process of MCS is detailed in Algorithm 1.

Algorithm 1: MCS

Input: CSI matrix $\mathbf{H}$, the threshold θ_{UE}
Output: Masked CSI matrix $\mathbf{H}_m$, mask matrix $\mathbf{M}$
`/* Calculate the score of each element and the total score */`;
current score $sum_c \leftarrow 0$, total score $sum_t \leftarrow 0$, flag $f \leftarrow 0$;
for $i \leftarrow 0$ **to** *length of* $\mathbf{H}$ **do**
  for $j \leftarrow 0$ **to** *width of* $\mathbf{H}$ **do**
    Calculate $score_{i,j}$ according to (10);
    $sum_t \leftarrow sum_t + score_{i,j}$;
  end
end
`/* Select important values that will not be masked */`;
Sort the matrix of $score_{i,j}$ in descending order and get the list **scores**;
Create empty index list $list_i$;
while *current score* $<$ *total score* $\times\theta_{UE}$ **do**
  current score $\leftarrow$ current score $+$ **scores**$[flag]$;
  Append the index of **scores**$[flag]$ in $\mathbf{H}$ to $list_i$;
  $f \leftarrow f + 1$;
end
`/* Build masked CSI matrix */`;
Create a zero matrix $\mathbf{M}$ with the same size of $\mathbf{H}$;
foreach *index in* $list_i$ **do**
  $\mathbf{M}[index] \leftarrow 1$;
end
$\mathbf{H}_m \leftarrow \mathbf{H} \odot \mathbf{M}$;

V. Transmitting the Important Values using AQ-MH

After selecting the important values in a CSI matrix using the MCS algorithm, the next step is to convert them into a binary sequence and transmit them to the BS through the wireless channel. Transmitting the positions and values of the important values is equivalent to transmitting the masked CSI matrix $\mathbf{H}_m$ produced by the MCS algorithm. Although $\mathbf{H}_m$ has the same shape as $\mathbf{H}$, it is highly sparse, meaning a large proportion of its elements are zeros. As a result, transmitting this highly sparse matrix requires far fewer bits compared to the full matrix $\mathbf{H}$. This section discusses how to transmit $\mathbf{H}_m$ while reducing communication overhead as much as possible.

By scanning each row of $\mathbf{H}_m$ from left to right and iterating through all rows from top to bottom, the non-zero values are collected to form a sequence of important values, $\mathbf{l}$. The sequence $\mathbf{l}$ and the mask matrix $\mathbf{M}$ are then separately encoded

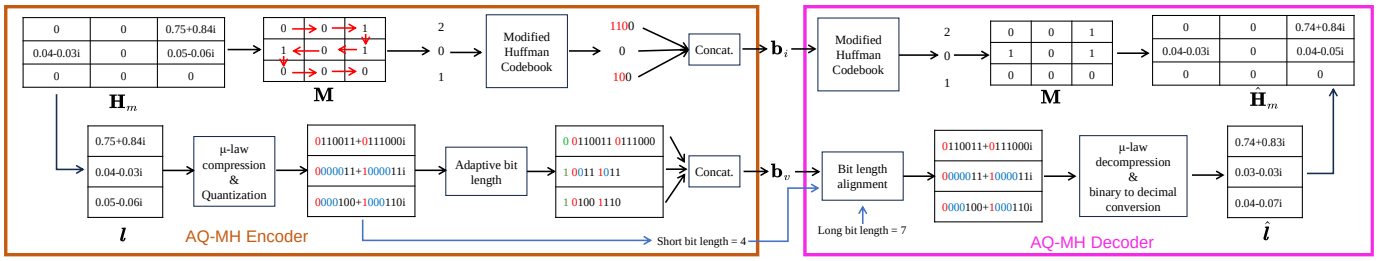

Fig. 3. An example of transmitting the important values using the AQ-MH algorithm.

into bit streams $\mathbf{b}_v$ and $\mathbf{b}_i$, using the adaptive bit length quantization method and the modified Huffman encoding method, respectively. We refer to these two methods collectively as the AQ-MH method. The following sections describe in detail how $\mathbf{l}$ and $\mathbf{M}$ are processed separately, followed by an integrated algorithm description of AQ-MH.

A. The Adaptive Bit Length Method for Encoding and Decoding the Sequence of Important Values

The important values in $\mathbf{l}$ are complex-valued, and each real and imaginary part undergoes μ-law compression followed by quantization using a predefined long bit length q_L. As mentioned in Sec. II-A, each CSI matrix is scaled to the range [-1, 1], meaning the maximum possible absolute value for each real or imaginary part is 1. Therefore, the quantization interval is $1/2^{q_L-1}$, with the first bit used to indicate the sign of the value.

A binary sequence representing a real or imaginary value consists of three parts. The first part is the sign bit, which identifies whether the value is positive or negative. The second part consists of a series of zeros that appear before the first occurrence of a "1". These zeros are included only to satisfy the fixed bit length q_L and do not represent the value itself. The third part consists of the useful bits, starting from the first "1" to the end, which represent the quantized value.

It is important to note that the second part of each binary sequence, consisting of the zeros before the first "1", can be removed. However, this removal leads to a variable bit length for each value. To address this, a short bit length q_S can be chosen. If the bit length of both the real and imaginary parts of a value, after removing the second part, is shorter than q_S, then q_S will be used as the bit length for that value. Otherwise, the long bit length q_L will still be used. For each value, an additional bit is appended to indicate whether q_L or q_S is being used. The choice of q_S depends on the overall bit savings achieved across all values in $\mathbf{l}$. By testing different candidate values for q_S, the one that results in the greatest bit savings is selected. This process is referred to as the adaptive bit length method.

Each bit sequence representing the complex-valued values in $\mathbf{l}$ is concatenated to form the complete bit sequence $\mathbf{b}_v$. When decoding $\mathbf{b}_v$, both the long and short bit lengths, q_L and q_S, need to be known. By identifying whether the first bit in $\mathbf{b}_v$ is 0 or 1, the bit length of the current value can be determined as either short or long. The corresponding bit segment is then processed using dequantization and μ-law decompression operations to recover the value. After that, the next bit is identified as 0 or 1, and this process repeats until the entire sequence is decoded. This procedure produces a recovered sequence of important values, $\hat{\mathbf{l}}$. The full process is illustrated in the lower branch of Fig. 3.

B. The Modified Huffman-based Method for Encoding and Decoding the Mask Matrix

Since the mask matrix $\mathbf{M}$ is a highly sparse binary matrix, we choose to encode the relative indices of the ones in $\mathbf{M}$. Starting from the top-left corner, each value is scanned in a snake-like pattern, and the relative distance of each "1" is recorded. The relative distance ranges from 0 to 1024. To encode these relative distances, the modified Huffman codebook, as proposed in [38], is applied. The resulting encoded bit sequences are then concatenated to form the final bit sequence $\mathbf{b}_i$.

Because the modified Huffman codebook is uniquely decodable, $\mathbf{b}_i$ can be used to fully reconstruct the mask matrix $\mathbf{M}$ during decoding. The entire process, including the encoding and decoding of $\mathbf{M}$ using the modified Huffman-based method, is shown in the top branch of Fig. 3.

After obtaining the sequence of quantized important values $\hat{\mathbf{l}}$ and the mask matrix $\mathbf{M}$, the recovered masked CSI matrix $\hat{\mathbf{H}}_m$ is generated by sequentially placing each value from $\hat{\mathbf{l}}$ into the "1" positions in $\mathbf{M}$. The encoder and decoder processes for AQ-MH are described in detail in Algorithm 2 and Algorithm 3.

VI. Generating the Masked Values with TPMVNet

The TPMVNet, located at the BS side, is designed to generate the values at the "0" positions in $\hat{\mathbf{H}}_m$, which correspond to the predictable and unimportant values, as discussed in Sec. IV-A, that are discarded by the UE during transmission. The output of TPMVNet, $\hat{\mathbf{H}}$, serves as the reconstructed CSI matrix in the ITUG framework. This section covers the mechanism, network structure, training process, and deployment of TPMVNet.

A. Generation Mechanism: the Masking and Completion Tasks

Essentially, the input to TPMVNet is a masked image, as the data format of the CSI matrix closely resembles a 2D image. The task of TPMVNet is to fill in and recover the masked values based on the unmasked pixels. This mechanism

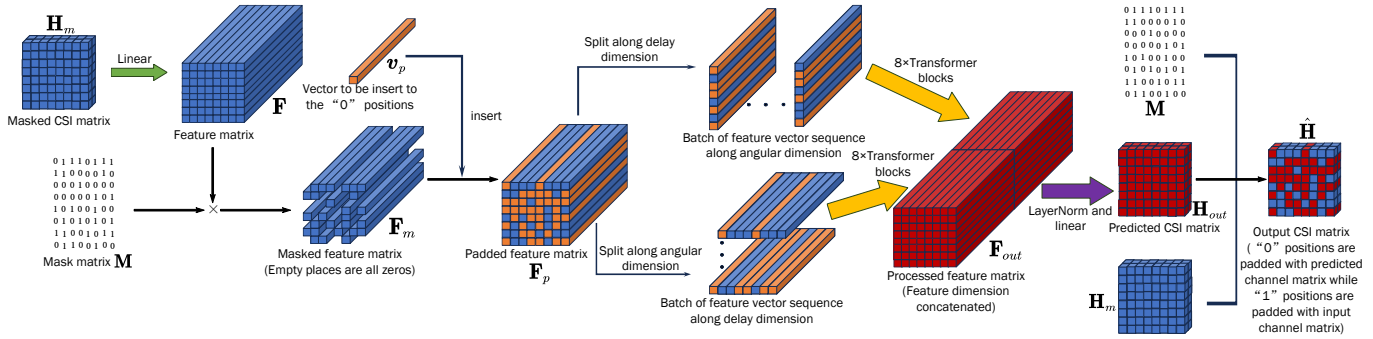

Fig. 4. The illustration of all details of TPMVNet.

Algorithm 2: AQ-MH Encoder

Input: Masked CSI matrix $\mathbf{H}_m$, the long quantization bit length q_L

Output: Bit sequences of important values $\mathbf{b}_v$ and their positions $\mathbf{b}_i$

/* Separate the mask matrix $\mathbf{M}$ and the sequence of important values $\mathbf{l}$ from $\mathbf{H}_m$ */;

/* Encode $\mathbf{l}$ */;

Produce μ-law compression and quantization with the bit length of q_L;

total save bits $q_t \leftarrow 0$;

for $q_S \leftarrow q_L - 1$ **to** 1 **do**

  current save bits $q_c \leftarrow 0$;

  foreach v_l *in* $\mathbf{l}$ **do**

    if q_S *can be applied to quantize and encode* v_l **then**

      $q_c \leftarrow q_c + 2(q_L - q_S)$;

    end

  end

  if $q_c > q_t$ **then**

    $q_t \leftarrow q_c$;

    Select current q_S as the picked one;

  end

end

Use the finally picked q_S to quantize and encode the available values;

Concatenate each bit sequence representing value to form $\mathbf{b}_v$;

/* Encode $\mathbf{M}$ */;

Get the relative distance of "1"s in $\mathbf{M}$;

Encode each distance with the modified Huffman codebook proposed in [38];

Concatenate each bit sequence to form $\mathbf{b}_i$;

Algorithm 3: AQ-MH Decoder

Input: Bit sequences of important values $\mathbf{b}_v$ and their positions $\mathbf{b}_i$, long bit length q_L, short bit length q_S

Output: The recovered masked CSI matrix $\hat{\mathbf{H}}_m$

/* Decode $\mathbf{b}_v$ */;

Decode each value from $\mathbf{b}_v$ using the bit lengths q_L and q_S;

Reconstruct the sequence of important values $\hat{\mathbf{l}}$;

/* Decode $\mathbf{b}_i$ */;

Decode each relative distance from $\mathbf{b}_i$ using the modified Huffman codebook;

Reconstruct the mask matrix $\mathbf{M}$ using the decoded relative distances;

Generate $\hat{\mathbf{H}}_m$ with $\hat{\mathbf{l}}$ and $\mathbf{M}$;

is quite similar to the masking and completion tasks, which have been used as a pre-training task in early large language models, especially BERT [41], and currently exploration of large image models, especially MAE [42]. The success of the masking-completion paradigm has demonstrated its ability to train high-performance foundation models that are well-suited for a variety of downstream tasks.

However, according to the results presented in [42], if certain important information in the input image is masked, the trained network cannot recover it out of thin air. In other words, the MAE network can only restore the masked areas based on the available information and the inherent continuity of image data. This is why we choose to transmit important values in the CSI matrices because once they are masked, the network will not be able to recover them.

B. The Structure of TPMVNet and the Training Process

When training the TPMVNet model, it is not yet deployed in the ITUG framework, and the input is directly the masked CSI matrix $\mathbf{H}_m$. The TPMVNet model is tasked with outputting a reconstructed CSI matrix $\hat{\mathbf{H}}$ that is as close as possible to the original matrix $\mathbf{H}$. Next, we describe the structure of TPMVNet by outlining the forward propagation process during training. We will also introduce the loss function used in the training process.

1) Data preparing before processed by Transformer layers: First, a linear fully connected layer is used to transform $\mathbf{H}_m$ to the feature matrix $\mathbf{F} \in \mathbb{R}^{N_f \times N_t \times N_L}$, where N_L represents the dimension of a feature vector. Then the masked feature matrix $\mathbf{F}_m \in \mathbb{R}^{N_f \times N_t \times N_L}$ is acquired by calculating the Hadamard product between $\mathbf{F}$ and the mask matrix $\mathbf{M}$, which is formulated as

$$\mathbf{F}_m = \mathbf{F} \odot \mathbf{M}. \tag{9}$$

After this operation, the indices of "0" in $\mathbf{M}$ correspond to all-zero vectors in $\mathbf{F}_m$. A vector $\mathbf{v}_p \in \mathbb{R}^{N_L}$ is generated for replacing all the masked vectors in $\mathbf{F}_m$. After this operation, the padded feature matrix $\mathbf{F}_p \in \mathbb{R}^{N_f \times N_t \times N_L}$ is obtained, where all the masked positions are padded with the same vector $\mathbf{v}_p$.

2) Using Transformer layers to predict the masked values of CSI matrix: The Transformer layers process data in the form of a sequence of feature vectors, while $\mathbf{F}_p$ is in the form of a feature vector matrix. To enable the Transformer layers to process $\mathbf{F}_p$, $\mathbf{F}_p$ is split row-wise and column-wise to form a set of angular domain feature vector sequences and a set of delay domain feature vector sequences. Then 8 layers of Transformer block are applied to process them. The processed sequences are reshaped to the shape of $\mathbf{F}_p$ and are concatenated along the feature dimension to produce the proposed feature matrix $\mathbf{F}_{out} \in \mathbb{R}^{N_f \times N_t \times 2N_L}$. Finally, the feature dimension of $\mathbf{F}_{out}$ is compressed by a LayerNorm layer and a fully connected layer and gets the predicted CSI matrix $\mathbf{H}_{out} \in \mathbb{R}^{N_f \times N_t \times 2}$.

3) Post-processing: In $\mathbf{H}_{out}$, all values are generated by the model. To keep the important values that are not masked in the origin CSI matrix $\mathbf{H}$ stable, the values in $\mathbf{H}_{out}$ with the same indices as the "1"s in the mask matrix $\mathbf{M}$ should be replaced by the values at the corresponding indices in $\hat{\mathbf{H}}_m$. The modified output matrix is considered as the finally reconstructed CSI matrix $\hat{\mathbf{H}}$. In $\hat{\mathbf{H}}$, the important values that are transmitted from the origin CSI matrix at UE stay the same value and position as $\mathbf{H}$, while the masked positions are padded with the corresponding values predicted by the TPMVNet.

4) Definition of Loss Function and the Training of TP-MVNet: When training the TPMVNet, the encoding process at UE and the decoding process at BS are not included so that the input of the TPMVNet is $\mathbf{H}_m$ and the important values are not quantized so there is no quantization noise. Therefore, the important values in the reconstructed $\hat{\mathbf{H}}$ are identical to those in the origin CSI matrix $\mathbf{H}$. The loss function is defined by calculating the mean square error (MSE) between the masked values in $\mathbf{H}$ and $\hat{\mathbf{H}}$, which is formulated as

$$\mathcal{L} = \mathbb{E}\left[\frac{1}{\sum\limits_{m_i \in \mathbf{M}} m_i} \sum_{j \in indices\ in\ \mathbf{M}}^{where\ m_j=1} \sqrt{(h_j - \hat{h}_j)^2}\right]. \tag{10}$$

In the backward propagation, the parameters that need to be updated include the 8 layers of the Transformer block, the initial feature embedding fully connected layer, the vector $\mathbf{v}_p$ used to replace the masked positions, as well as the LayerNorm and fully connected layer at the end. The illustration of the proposed TPMVNet, including all the details mentioned above, is in Fig. 4.

C. The Deployment of TPMVNet

When TPMVNet completes training and is deployed, there are two main differences compared to its training phase. The first difference is that the input changes to $\hat{\mathbf{H}}_m$, which is the output from the AQ-MH decoder described in Sec. V. The key distinction between $\mathbf{H}_m$ and $\hat{\mathbf{H}}_m$ lies in the fact that the important values in $\hat{\mathbf{H}}_m$ are quantized. The second difference is that the number of important values may vary, depending on the threshold θ_{UE} described in Sec. IV-B, which the UE uses to determine the proportion of important values to transmit.

It is important to note that during TPMVNet training, the proportion of important values in $\mathbf{H}_m$ is fixed across all samples in the training dataset. This fixed threshold is referred to as the training data threshold θ_{train}. Different values of θ_{train} produce different versions of TPMVNet. In other words, each TPMVNet is trained with a constant θ_{UE}. However, during deployment, the θ_{UE} of the input for a particular TPMVNet does not need to match its corresponding θ_{train}, meaning that a TPMVNet is capable of handling varying conditions in the input $\hat{\mathbf{H}}_m$.

VII. Experimental Results

A. Channel Settings

We use the QuaDRiGa channel model [43] to generate channel matrices in three scenarios: LOS (Line-of-Sight), NLOS (Non-Line-of-Sight), and O2I (Outdoor-to-Indoor). For each scenario, a BS equipped with a 32×1 Uniform Linear Array (ULA) antenna array is configured. The BS operates at a central frequency of 2.655GHz with a bandwidth of 70MHz. The BS height is 10 meters. Within the $100m \times 100m$ coverage area of the BS, 100,000 positions are randomly chosen, and the CSI matrices at these positions are generated. At each position, it is assumed that there is a UE equipped with an omnidirectional antenna. The UEs uniformly sample 32 points across the frequency bandwidth and then, through a 2D-DFT, obtain 32×32 angle-delay domain channel matrices. The CSI matrix processing procedure follows Section II-A. Therefore, for each scenario, there are 100,000 CSI matrices of size $\mathbb{C}^{32\times32}$.

B. The Preparation of Neural Network Models

To evaluate the effectiveness of the proposed ITUG framework, we implement the TPMVNet within the ITUG framework and also compare its performance against several high-performance models that are commonly employed in autoencoder-based frameworks.

1) TPMVNet: The training and deployment process of TP-MVNet have been outlined in Sec. VI-B and Sec. VI-C. During training, we set the batch size to 128, the number of epochs to 200, and the learning rate to 0.0003. TPMVNet is trained in both NLOS and LOS scenarios, with the threshold θ_{train} (as mentioned in Sec. V-C) adjusted to control the masking ratio of the input data, producing different models. The trained TPMVNet models are named, for example, $\mathrm{TPMVNet}_{0.4}^{\mathrm{LOS}}$, indicating the model is trained in the LOS scenario with a threshold of $\theta_{train} = 0.4$.

2) Autoencoders: We train CRNet [4], ACRNet [5], and TransNet [6] in LOS and NLOS scenarios with different compression ratios γ. The compression ratio γ is defined as the ratio of the number of parameters in the compressed output to the number of parameters in the original input. When training these models, the loss function is the means square error (MSE), the learning rate is 0.0001, the batch size is

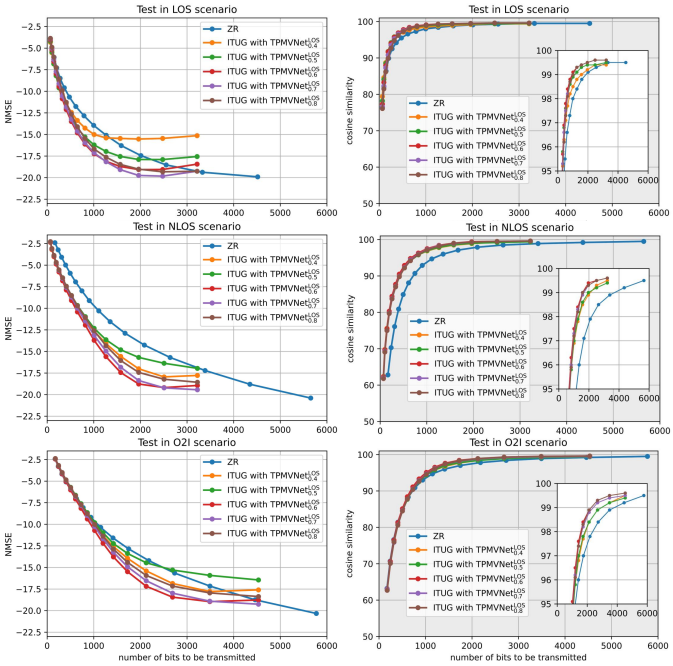

Fig. 5. Comparison of ZR and ITUG using TPMVNet trained in the LOS scenario, evaluated by NMSE and ρ under different communication overheads.

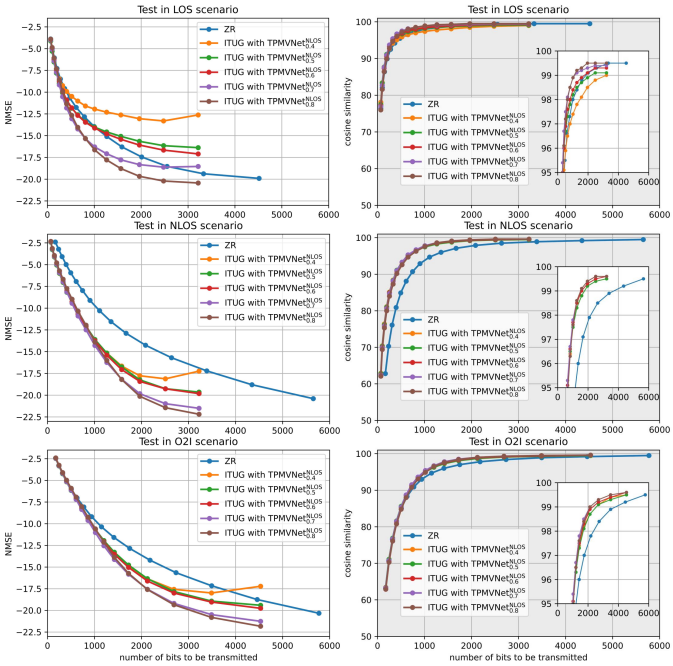

Fig. 6. Comparison of ZR and ITUG using TPMVNet trained in the NLOS scenario, evaluated by NMSE and ρ under different communication overheads.

256, and the number of epochs is 500. The trained models are named following the format $\mathrm{CRNet}_{1/4}^{\mathrm{LOS}}$, indicating that CRNet is trained in the LOS scenario with a compression ratio of 1/4.

When deploying these models in the AE-based framework, the latent code $\mathbf{s}$ output by the encoder at the UE must be quantized and encoded before being transmitted to the BS. To ensure optimal performance, the pre-trained models, along with the encoding and decoding modules for the latent code, are fine-tuned within the same training scenario. All autoencoder models referenced in the following sections are the fine-tuned versions.

C. Performance Indicators

We select two indicators to evaluate the reconstruction accuracy of different CSI feedback methods. The first is the normalized mean square error (NMSE), which is formulated as

$$\mathrm{NMSE} = 10\log[\frac{1}{N_{test}}\sum_{i=1}^{N_{test}}\frac{\|\hat{\mathbf{H}}-f(\hat{\mathbf{H}})\|_2^2}{\|\hat{\mathbf{H}}\|_2^2}], \qquad (11)$$

where $\hat{\mathbf{H}}$ denotes the recovered $\mathbf{H}$, and N_{test} represent the total sample count in the test set. The second is the cosine similarity ρ, which is used to gauge the precoding performance. The cosine similarity, ρ, is expressed as

$$\rho = \mathbb{E}\frac{1}{N_c}\sum_{m=1}^{N_c}\frac{|\hat{\mathbf{h}}_m^H\mathbf{H}_m|}{\|\hat{\mathbf{h}}_m\|_2\|\mathbf{h}_m\|_2}, \qquad (12)$$

where $\hat{\mathbf{h}}_m$ signifies the reconstructed channel vector for the m-th frequency sample point. When the BS uses $\mathbf{v}_m = \hat{\mathbf{h}}_m/\|\hat{\mathbf{h}}_m\|_2$ as a beamforming vector, the cosine similarity can be indicative of the precoding gain.

D. Comparison of ITUG and Zero-replacement Method

In this subsection, we compare the performance of our proposed ITUG framework with the Zero-Padding (ZR) framework for CSI feedback, as discussed in the related work [38] which is mentioned in Sec. I and Sec. 3. The ZR framework also reconstructs the CSI matrix by transmitting only a small portion of the values from the original matrix. However, unlike the ITUG framework, it does not recover the untransmitted values, and its selection algorithm and transmission scheme differ from our approach. We implement the ZR framework on our dataset and obtain performance indicators, including NMSE and ρ, for the reconstructed CSI matrix and the original one. The detailed comparison results are presented in the following sections.

1) Communication Overhead Adjustment: Both the ITUG and ZR frameworks transmit a proportion of values from the CSI matrix, allowing for the adjustment of communication overhead by modifying the number of transmitted values. In the ITUG framework, we define the threshold θ_{UE}, which the UE uses to determine the proportion of important values to be transmitted, thereby controlling the communication overhead. For the ZR framework, as described in its original operation in [38], communication overhead is adjusted by selecting a fraction of all values, similar to the compression ratio γ in AE-based methods. However, since the transmission of a fixed number of values can lead to significant variations in reconstruction performance across different samples, we also introduce a threshold for ZR. This threshold is based solely on the amplitude of the values, while the selection process remains the same as in ITUG.

We conduct tests using 16 equally spaced θ_{UE} values ranging from 0.15 to 0.9 in three different channel scenarios:

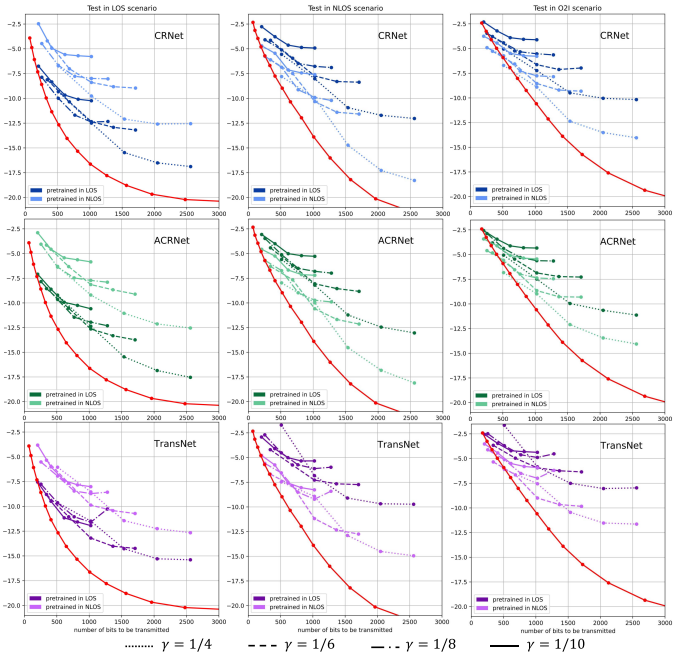

Fig. 7. Comparison of different autoencoder models and ITUG equipped with $\mathrm{TPMVNet}_{0.8}^{\mathrm{NLOS}}$ evaluated by NMSE tested in different scenarios.

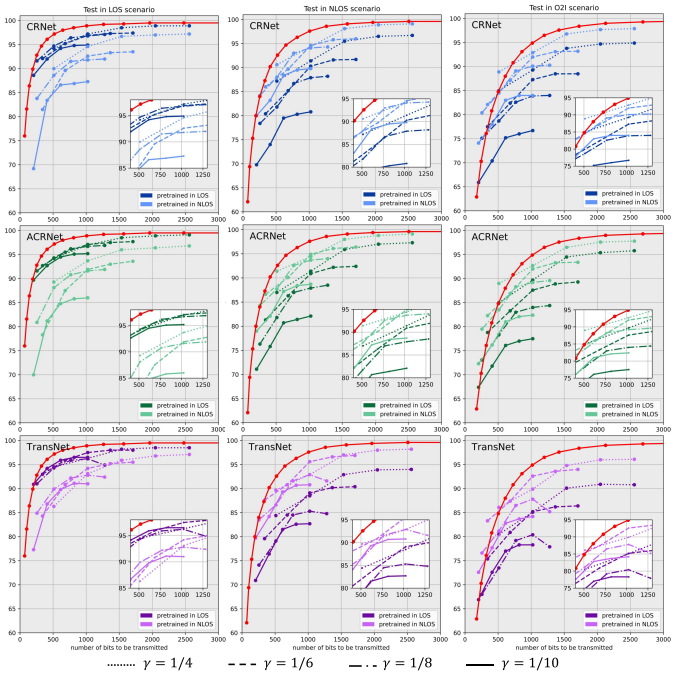

Fig. 8. Comparison of different autoencoder models and ITUG equipped with $\mathrm{TPMVNet}_{0.8}^{\mathrm{NLOS}}$ evaluated by ρ tested in different scenarios.

LOS, NLOS, and O2I. In each scenario, 10,000 samples are tested, with the quantization bit length set to $q_L = 7$. The average communication overhead and corresponding performance metrics are computed and displayed on the x-axis and y-axis, respectively, in Fig. 5 and Fig. 6.

2) Comparison of ZR and ITUG with TPMVNet Trained in the LOS Scenario: In Fig. 5, we compare the performance of ZR and ITUG with TPMVNets trained in the LOS scenario, using NMSE and ρ as metrics. The results show that TPMVNet trained with a higher threshold θ_{train} leads to better reconstruction accuracy. When comparing ITUG with the better-performing $\mathrm{TPMVNet}_{0.8}^{\mathrm{LOS}}$ and the ZR method, we observe that as communication overhead increases, or as more values are transmitted, ITUG achieves superior reconstruction accuracy faster than ZR. This performance gain of ITUG over ZR highlights the advantage of TPMVNet in reconstructing the masked matrix at the BS side, in contrast to ZR, which directly uses the masked matrix as the final reconstruction result. Although ZR eventually reaches better performance, it does so with significantly higher communication overhead. Each point along the lines corresponds to the same threshold, and it is evident that the ZR line is consistently to the right of the ITUG lines. This means that for each threshold, the ZR method typically requires more transmission bits. This demonstrates that the ITUG framework's transmission scheme is more efficient in reducing communication overhead.

3) Comparison of ZR and ITUG with TPMVNet Trained in the NLOS Scenario: We also compare the performance of ZR and ITUG with TPMVNets trained in the NLOS scenario in Fig. 6. From the test results across the LOS, NLOS, and O2I scenarios, we observe that ITUG with $\mathrm{TPMVNet}_{0.8}^{\mathrm{NLOS}}$ outperforms $\mathrm{TPMNVet}_{0.8}^{\mathrm{LOS}}$, achieving consistently lower communication overhead and better reconstruction accuracy in terms of NMSE compared to the ZR method in all these three scenarios. This result highlights the exceptional performance and generalization ability of $\mathrm{TPMVNet}_{0.8}^{\mathrm{NLOS}}$. Although its superiority in terms of ρ is not as pronounced, it still demonstrates competitive performance. Consequently, we select $\mathrm{TPMVNet}_{0.8}^{\mathrm{NLOS}}$ as the representative model to be deployed in the ITUG framework for subsequent experiments.

E. Comparison of ITUG and Autoencoder Models

1) The Autoencoder Models for Latent Code Transmission: We further compare the reconstruction performance of our proposed ITUG framework equipped with $\mathrm{TPMVNet}_{0.8}^{\mathrm{NLOS}}$ against classic autoencoder-based CSI feedback methods. As detailed in Sec. VII-B2, we train CRNet, ACRNet, and TransNet models in the LOS and NLOS scenarios. The quantization and dequantization modules for the latent code $\mathbf{s}$ are adapted from the approach in [44]. For each pre-trained autoencoder model, we select the quantization bit values $q_s = 1, 2, 3, 4, 5$ and fine-tune these 5 versions, with each one representing a different bit length for quantizing the latent code. The communication overhead for processing a single CSI matrix $\mathbf{H}$ sample is calculated as

$$c_{AE} = 2048 \times \gamma \times q_s, \tag{13}$$

where 2048 denotes the total number of real-values components (real and imaginary parts) in $\mathbf{H} \in \mathbb{C}^{32\times 32}$.

2) The Arrangement of Result Figure: The reconstruction accuracy results are illustrated in Fig. 7 and 8 using the performance metrics NMSE and ρ, respectively. These figures consist of nine sub-charts arranged in a 3×3 grid. Each row corresponds to a specific category of autoencoder model, while each column represents a particular test scenario (e.g.

LOS, NLOS, O2I). In each sub-chart, the red line represents the performance curve of the ITUG framework equipped with $\mathrm{TPMVNet}_{0.8}^{\mathrm{NLOS}}$, which is identical to that shown in Fig. 6. We use a consistent color scheme to indicate the performance of different autoencoder models, and distinguish whether the model is trained in the LOS or NLOS scenario by using darker or lighter shades of the same color. Specifically, the darker shade represents models trained in the LOS scenario, while the lighter shade corresponds to models trained in the NLOS scenario. To differentiate models with varying compression ratio γ, distinct line styles are employed. Every curve, except the red one, describes the performance of a particular pre-trained autoencoder model version. The five points on each curve correspond to the fine-tuned versions with quantization bit lengths $q_s = 1, 2, 3, 4, 5$ for the latent code $\mathbf{s}$, arranged from left to right. These quantization bit lengths are converted into the corresponding communication overhead c_{AE} calculated as (13), representing the total number of bits required for transmission.

3) Performance and Generalization Ability Across Different Scenarios: In the first column of Fig. 7 and 8, the performance of the autoencoder models trained in the LOS scenario clearly surpasses those trained in the NLOS scenario. This highlights the impact of performance degradation in autoencoder models when there is a mismatch between the training and deployment channel scenarios. Additionally, while the ITUG method with $\mathrm{TPMVNet}_{0.8}^{\mathrm{NLOS}}$ also faces a scenario mismatch when trained in NLOS but tested in LOS, it still achieves exceptional reconstruction performance, outperforming even the autoencoder models that are trained specifically in the LOS scenario. This demonstrates the superiority of our proposed ITUG framework in terms of both performance and generalization ability.

In the second column of Fig. 7 and 8, where performance in the NLOS scenario is depicted, the results show a reverse trend compared to the LOS scenario in the first column: autoencoder models trained in the NLOS scenario outperform those trained in the LOS. This phenomenon further confirms the performance degradation problem in autoencoder models when then encounter mismatched scenarios. In this case, the ITUG framework with $\mathrm{TPMVNet}_{0.8}^{\mathrm{NLOS}}$ consistently outperforms all the autoencoder models, reinforcing its robustness and effectiveness across different scenarios.

In the third column of Fig. 7 and Fig. 8, both the ITUG and autoencoder models are evaluated in the O2I scenario, which is novel to all deep learning models in the framework. Here, autoencoders trained in the NLOS scenario slightly outperform those trained in LOS, suggesting that the O2I scenario is more similar to NLOS than to LOS. However, the performance gap between models trained in NLOS versus LOS is less pronounced than in the previous two columns, which can indirectly indicate that both pre-trained models exhibit more or less performance degradation. When considering ITUG's performance relative to the autoencoders, ITUG shows a notably larger performance advantage, especially as communication overhead increases. This larger margin indicates that ITUG is expected to generalize and perform better than autoencoders when adapting to new scenarios, showcasing its robustness and adaptability.

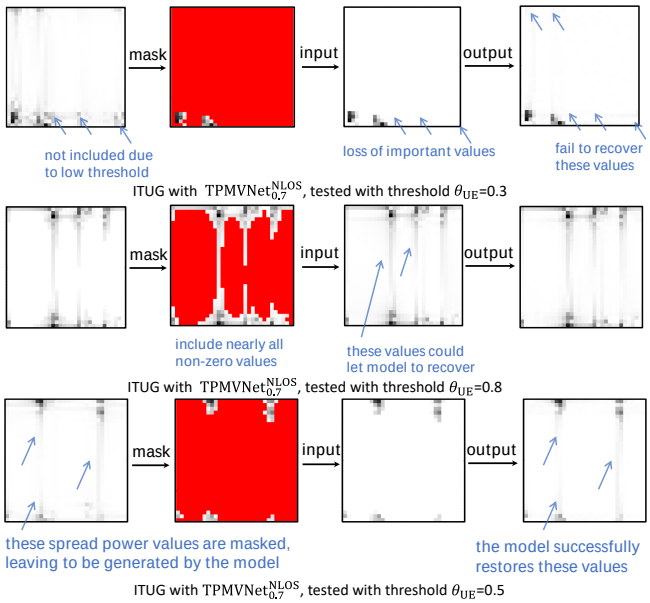

Fig. 9. Visualization of UE-side important value selection, illustrating input and output CSI matrices of $\mathrm{TPMVNet}_{0.7}^{\mathrm{NLOS}}$ under three θ_{UE} levels (low, high, and medium).

However, it is worth noting that when the communication overhead is extremely low, the performance of ITUG is not as good as that of the autoencoders with a larger compression ratio γ (e.g. $\gamma = 1/10$) and a shorter quantization bit length (e.g. $q_s = 1$) when tested in the O2I scenario. This phenomenon also appears in tests conducted in the LOS and NLOS scenarios, where the performance advantage of ITUG over autoencoders narrows significantly, and may even disappear entirely. However, fortunately, in such cases, both ITUG and the autoencoder models exhibit poor reconstruction accuracy, which is unacceptable for real deployment. Overall, it can be concluded that ITUG demonstrates better reconstruction and generalization performance in most scenarios.

F. Exploring Ideal Conditions for ITUG Performance

In Figs. 5 and 6, we observe that under a large communication overhead, ITUG's performance advantage narrows compared to the Zero-Padding method. Similarly, Figs. 7 and 8 show that under a small communication overhead, ITUG's performance lead also diminishes or even falls below that of the autoencoder models. These results suggest that when the communication overhead is either too small or too large, ITUG's performance advantage over other CSI feedback methods is reduced. Given that communication overhead is directly related to the threshold θ_{UE} for selecting important values at the UE side, this indicates that when θ_{UE} is set too low or too high, TPMVNet's effectiveness in generating masked values declines. To explore this further, we selected three threshold values, $\theta_{UE} = 0.3$, 0.8, and 0.5, representing a small, large, and moderately suitable threshold, respectively, and applied them to three typical CSI matrix samples. The visualization results are shown in Fig. 9.

When $\theta_{UE} = 0.3$, in the first row of Fig. 9, the threshold is too restrictive, causing some genuinely important values to

TABLE I
COMPUTATIONAL COMPLEXITY (FLOPS) OF ITUG, ZR, AND THE AUTOENCODER MODELS AT THE UE SIDE. M: MILLION

ITUG	0.064M	ZR	0.034M		$\gamma = 1/4$	$\gamma = 1/6$	$\gamma = 1/8$	$\gamma = 1/10$
				CRNet	13.4M	12.7M	12.3M	12.1M
				ACRNet	2.7M	2.0M	1.7M	1.4M
				TransNet	36.2M	35.5M	35.2M	35.0M

be masked. As previously described, the TPMVNet model is unable to recover these important values. Consequently, both the masked CSI matrix $\mathbf{H}_m$, the quantized matrix $\hat{\mathbf{H}}_m$, and the reconstructed matrix $\hat{\mathbf{H}}$ are missing some important values, resulting in almost no performance gain from using the TPMVNet model. Additionally, the baseline performance of ITUG is not competitive due to excessive information loss.

When $\theta_{UE} = 0.8$, in the second row of Fig. 9, the threshold is too loose, causing a large number of predictable values to be included in $\hat{\mathbf{H}}_m$ or $\mathbf{H}_m$ and thus visible to the TPMVNet model. Consequently, the model only needs to predict those unimportant values, which are intuitively close to zero. As a result, the output of the model $\hat{\mathbf{H}}$ is not significantly different from its input, resulting in almost no performance as well.

Only when $\theta_{UE} = 0.5$, as shown in the third row of Fig. 9, is the threshold large enough to ensure that almost all important values are visible to the TPMVNet model, while still being small enough to mask almost all the predictable values that remain for the model to generate. In this case, the model's output is clearly closer to the original CSI matrix than its input. Therefore, when the threshold θ_{UE} for selecting important values is accurately chosen—meaning it is both large enough to capture the important values and small enough to exclude predictable ones, while keeping the communication overhead within a tolerable range—the TPMVNet can deliver the highest performance gain, leading to the best-performing ITUG framework.

G. Complexity Comparison

After comparing the performance between our proposed ITUG framework and the ZR method, which also uses partial value transmission, as well as classical autoencoder-based networks for CSI feedback, it is essential to examine the computational complexity of these methods, particularly on the cost-sensitive UE side. We collect the Floating Point Operations (FLOPs) required by each method at the UE side. As for the BS side, given that the BS is generally resource-rich in terms of power and energy, the computational cost is considered less critical; therefore, we omit complexity considerations for these methods at the BS side. Table I presents the FLOPs comparison for these methods at the UE side.

From Table I, it is evident that the autoencoder networks exhibit significantly higher computational complexity, with even the lightest ACRNet requiring over 20 times more FLOPs than either ITUG or ZR. This disparity arises from the fully connected and CNN layers within these networks, which are computationally dense. In contrast, the ITUG and ZR methods do not require neural networks on the UE side, resulting in much lower computational demands. Comparing ITUG to ZR, while ITUG involves twice the FLOPs of ZR, it is still considered a lightweight algorithm suitable for UE deployment.

According to industry technical reports and information in 3GPP TR 28.843 (CSI Table I) on CSI compression [45], encoder networks used by major players such as Huawei, Qualcomm, Apple, and Nokia typically require over 10 million FLOPs. In comparison, our proposed ITUG model requires fewer than 0.1 million FLOPs, which is significantly lower than the industry-accepted threshold. Additionally, with the FLOPS capacity of modern smartphone GPUs surpassing 2.1 TeraFLOPS ($\times 10^{12}$) [46], the computational demands of ITUG are well within the processing capabilities of contemporary mobile devices. This confirms that the computational complexity of ITUG aligns with industry standards and is highly suitable for deployment on modern smartphones.

VIII. CONCLUSION

This work introduces a novel mechanism for an AI-enhanced CSI feedback system, targeting the limitations of autoencoder-based CSI feedback networks, which often suffer performance drops when facing new channel scenarios. Departing from the conventional two-sided autoencoder design, we propose a novel framework named ITUG. In this framework, only the important values of a CSI matrix—representing a small fraction of the entire matrix—are transmitted, while the unimportant values are generated by a trained deep learning model at the BS side.

To identify the important values that significantly aid in CSI matrix reconstruction, we develop MCS, a scoring algorithm based on each value's amplitude and variation, selecting those with the highest scores. For efficient transmission of these values, we introduce the AQ-MH method, which includes an AQ-MH encoder located at the UE and a decoder at the BS. The AQ-MH method separately encodes the value and index of each critical value, employing adaptive quantization bit lengths and a modified Huffman encoding. To effectively reconstruct the untransmitted values, we design TPMVNet, a Transformer-based generation network capable of capturing the occurrence patterns of these unimportant values, leveraging the transmitted critical values as input.

We conducted extensive experiments comparing our proposed ITUG framework with various CSI feedback methods.

Experimental results indicate that a single TPMVNet model within the ITUG framework achieves superior reconstruction performance compared to both the Zero Padding method and autoencoder-based networks across multiple channel scenarios, as long as the communication overhead is neither excessively high nor extremely low. These results highlight ITUG's strong performance and generalization capabilities. Additionally, our analysis of computational complexity confirms that ITUG maintains an acceptable computational demand on the UE side, underscoring its deployability.

REFERENCES

[1] Z. Gao, L. Dai, Z. Wang, and S. Chen, "Spatially common sparsity based adaptive channel estimation and feedback for fdd massive mimo," *IEEE Transactions on Signal Processing*, vol. 63, no. 23, pp. 6169–6183, 2015.

[2] H. Son and Y.-H. Cho, "Analysis of compressed csi feedback in miso systems," *IEEE Wireless Communications Letters*, vol. 8, no. 6, pp. 1671–1674, 2019.

[3] C.-K. Wen, W.-T. Shih, and S. Jin, "Deep learning for massive mimo csi feedback," *IEEE Wireless Communications Letters*, vol. 7, no. 5, pp. 748–751, Oct. 2018.

[4] Z. Lu, J. Wang, and J. Song, "Multi-resolution CSI feedback with deep learning in massive MIMO system," in *ICC 2020 - 2020 IEEE International Conference on Communications (ICC)*, 2020, pp. 1–6.

[5] Z. Lu, X. Zhang, H. He, J. Wang, and J. Song, "Binarized aggregated network with quantization: Flexible deep learning deployment for CSI feedback in massive MIMO systems," *IEEE Trans. on Wireless Commun.*, vol. 21, no. 7, pp. 5514–5525, Jul. 2022.

[6] Y. Cui, A. Guo, and C. Song, "TransNet: Full attention network for CSI feedback in FDD massive MIMO system," *IEEE Wireless Commun. Lett.*, vol. 11, no. 5, pp. 903–907, May 2022.

[7] H. Li, B. Zhang, H. Chang, X. Liang, and X. Gu, "Cvlnet: A complex-valued lightweight network for csi feedback," *IEEE Wireless Commun. Lett.*, vol. 11, no. 5, pp. 1092–1096, 2022.

[8] J. Guo, C.-K. Wen, S. Jin, and G. Y. Li, "Convolutional neural network-based multiple-rate compressive sensing for massive mimo csi feedback: Design, simulation, and analysis," *IEEE Transactions on Wireless Communications*, vol. 19, no. 4, pp. 2827–2840, 2020.

[9] S. Mourya, S. Amuru, and K. K. Kuchi, "A spatially separable attention mechanism for massive mimo csi feedback," *IEEE Wireless Communications Letters*, vol. 12, no. 1, pp. 40–44, 2023.

[10] S. Tang, J. Xia, L. Fan, X. Lei, W. Xu, and A. Nallanathan, "Dilated convolution based csi feedback compression for massive mimo systems," *IEEE Transactions on Vehicular Technology*, vol. 71, no. 10, pp. 11 216–11 221, 2022.

[11] X. Chen, C. Deng, B. Zhou, H. Zhang, G. Yang, and S. Ma, "High-accuracy csi feedback with super-resolution network for massive mimo systems," *IEEE Wireless Communications Letters*, vol. 11, no. 1, pp. 141–145, 2022.

[12] 3GPP, "Technical report: 3rd generation partnership project; technical specification group radio access network; study on enhancement for data collection for nr and endc (release 17)," 3GPP, Technical Report TR 38.843, Sep 2023.

[13] J. Guo, C.-K. Wen, S. Jin, and X. Li, "Ai for csi feedback enhancement in 5g-advanced," *IEEE Wireless Communications*, vol. 31, no. 3, pp. 169–176, 2024.

[14] X. Li, J. Guo, C.-K. Wen, S. Jin, S. Han, and X. Wang, "Multi-task learning-based csi feedback design in multiple scenarios," *IEEE Transactions on Communications*, vol. 71, no. 12, pp. 7039–7055, 2023.

[15] Y. Cui, J. Guo, C.-K. Wen, and S. Jin, "Communication-efficient personalized federated edge learning for massive mimo csi feedback," *IEEE Transactions on Wireless Communications*, vol. 23, no. 7, pp. 7362–7375, 2024.

[16] C. Tan, D. Cai, F. Fang, Z. Ding, and P. Fan, "Federated unfolding learning for csi feedback in distributed edge networks," *IEEE Transactions on Communications*, pp. 1–1, 2024.

[17] J. Guo, Y. Zuo, C.-K. Wen, and S. Jin, "User-centric online gossip training for autoencoder-based csi feedback," *IEEE Journal of Selected Topics in Signal Processing*, vol. 16, no. 3, pp. 559–572, 2022.

[18] Z. Du, H. Li, L. Li, B. Zhang, Z. Liu, and X. Gu, "Training csi feedback model with federated learning in massive mimo systems," in *2023 8th IEEE International Conference on Network Intelligence and Digital Content (IC-NIDC)*, 2023, pp. 446–450.

[19] H. Xiao, W. Tian, W. Liu, and J. Shen, "Channelgan: Deep learning-based channel modeling and generating," *IEEE Wireless Communications Letters*, vol. 11, no. 3, pp. 650–654, 2022.

[20] H. Ye, L. Liang, G. Y. Li, and B.-H. Juang, "Deep learning-based end-to-end wireless communication systems with conditional gans as unknown channels," *IEEE Transactions on Wireless Communications*, vol. 19, no. 5, pp. 3133–3143, 2020.

[21] Z. Du, Z. Liu, H. Li, S. Fan, X. Gu, and L. Zhang, "Dig-csi: A distributed and generative model assisted csi feedback training framework," *IEEE Wireless Communications Letters*, vol. 13, no. 8, pp. 2035–2039, 2024.

[22] H. Zhang, Z. Lu, X. Zhang, and J. Wang, "Data augmentation for bridging the delay gap in dl-based massive mimo csi feedback," *IEEE Wireless Communications Letters*, vol. 13, no. 5, pp. 1315–1319, 2024.

[23] C. Jiang, J. Guo, C.-K. Wen, and S. Jin, "Multi-domain correlation-aided implicit csi feedback using deep learning," *IEEE Transactions on Wireless Communications*, vol. 23, no. 10, pp. 13 344–13 358, 2024.

[24] Z. Liu, L. Wang, L. Xu, and Z. Ding, "Deep learning for efficient csi feedback in massive mimo: Adapting to new environments and small datasets," *IEEE Transactions on Wireless Communications*, vol. 23, no. 9, pp. 12 297–12 312, 2024.

[25] B. Zhang, H. Li, X. Liang, X. Gu, and L. Zhang, "Multi-task training approach for csi feedback in massive mimo systems," *IEEE Communications Letters*, vol. 27, no. 1, pp. 200–204, 2023.

[26] B. Zhou, X. Yang, J. Wang, S. Ma, F. Gao, and G. Yang, "A low-overhead incorporation-extrapolation based few-shot csi feedback framework for massive mimo systems," *IEEE Transactions on Wireless Communications*, vol. 23, no. 10, pp. 14 743–14 758, 2024.

[27] J. Zeng, J. Sun, G. Gui, B. Adebisi, T. Ohtsuki, H. Gacanin, and H. Sari, "Downlink csi feedback algorithm with deep transfer learning for fdd massive mimo systems," *IEEE Transactions on Cognitive Communications and Networking*, vol. 7, no. 4, pp. 1253–1265, 2021.

[28] X. Zhang, J. Wang, Z. Lu, and H. Zhang, "Continuous online learning-based csi feedback in massive mimo systems," *IEEE Communications Letters*, vol. 28, no. 3, pp. 557–561, 2024.

[29] Y. Cui, J. Guo, C.-K. Wen, S. Jin, and S. Han, "Unsupervised online learning in deep learning-based massive mimo csi feedback," *IEEE Communications Letters*, vol. 26, no. 9, pp. 2086–2090, 2022.

[30] Y. Cui, J. Guo, Z. Cao, H. Tang, C.-K. Wen, S. Jin, X. Wang, and X. Hou, "Lightweight neural network with knowledge distillation for csi feedback," *IEEE Transactions on Communications*, vol. 72, no. 8, pp. 4917–4929, 2024.

[31] Z. Lu, X. Zhang, R. Zeng, and J. Wang, "Better lightweight network for free: Codeword mimic learning for massive mimo csi feedback," *IEEE Communications Letters*, vol. 27, no. 5, pp. 1342–1346, 2023.

[32] X. Li, J. Guo, C.-K. Wen, X. Geng, and S. Jin, "Facilitating ai-based csi feedback deployment in massive mimo systems with learngene," *IEEE Transactions on Wireless Communications*, vol. 23, no. 9, pp. 11 325–11 340, 2024.

[33] H. Xiao, W. Tian, W. Liu, J. Guo, Z. Zhang, S. Jin, Z. Shi, L. Guo, and J. Shen, "Knowledge-driven meta-learning for csi feedback," *IEEE Transactions on Wireless Communications*, vol. 23, no. 6, pp. 5694–5709, 2024.

[34] J. Guo, C.-K. Wen, M. Chen, and S. Jin, "Environment knowledge-aided massive mimo feedback codebook enhancement using artificial intelligence," *IEEE Transactions on Communications*, vol. 70, no. 7, pp. 4527–4542, 2022.

[35] P. Liang, J. Fan, W. Shen, Z. Qin, and G. Y. Li, "Deep learning and compressive sensing-based csi feedback in fdd massive mimo systems," *IEEE Transactions on Vehicular Technology*, vol. 69, no. 8, pp. 9217–9222, 2020.

[36] J. Wang, G. Gui, T. Ohtsuki, B. Adebisi, H. Gacanin, and H. Sari, "Compressive sampled csi feedback method based on deep learning for fdd massive mimo systems," *IEEE Transactions on Communications*, vol. 69, no. 9, pp. 5873–5885, 2021.

[37] Z. Wei, H. Liu, B. Li, and C. Zhao, "Joint massive mimo csi estimation and feedback via randomized low-rank approximation," *IEEE Transactions on Vehicular Technology*, vol. 71, no. 7, pp. 7979–7984, 2022.

[38] Y.-C. Lin, T.-S. Lee, and Z. Ding, "Training-free cost-efficient compression for massive MIMO channel state feedback," in *GLOBECOM 2023 - 2023 IEEE Global Communications Conference*, 2023, pp. 3391–3396.

[39] M. Nerini, V. Rizzello, M. Joham, W. Utschick, and B. Clerckx, "Machine learning-based csi feedback with variable length in fdd massive

mimo," *IEEE Transactions on Wireless Communications*, vol. 22, no. 5, pp. 2886–2900, 2023.

[40] H. Ju, S. Jeong, S. Kim, B. Lee, and B. Shim, "Transformer-assisted parametric csi feedback for mmwave massive mimo systems," *IEEE Transactions on Wireless Communications*, pp. 1–1, 2024.

[41] J. Devlin, M.-W. Chang, K. Lee, and K. Toutanova, "BERT: Pre-training of deep bidirectional transformers for language understanding," in *Proceedings of the 2019 Conference of the North American Chapter of the Association for Computational Linguistics: Human Language Technologies, Volume 1 (Long and Short Papers)*, Jun. 2019.

[42] K. He, X. Chen, S. Xie, Y. Li, P. Dollár, and R. Girshick, "Masked autoencoders are scalable vision learners," in *2022 IEEE/CVF Conference on Computer Vision and Pattern Recognition (CVPR)*, 2022.

[43] S. Jaeckel, L. Raschkowski, K. Börner, L. Thiele, F. Burkhardt, and E. Eberlein, "QuaDRiGa-quasi deterministic radio channel generator, user manual and documentation," *Fraunhofer Heinrich Hertz Institute, Tech. Rep. v2.8.1*, 2023.

[44] Z. Liu, L. Zhang, and Z. Ding, "An efficient deep learning framework for low rate massive mimo csi reporting," *IEEE Transactions on Communications*, vol. 68, no. 8, pp. 4761–4772, 2020.

[45] "Study on artificial intelligence (AI)/machine learning (ML) for NR air interface (release 18)," 3GPP, Technical Report TR 38.843, Sep 2023, [Online]. Available: http://www.3gpp.org.

[46] NanoReview. (2023) Smartphone processors ranking. Accessed: Dec. 28, 2023. [Online]. Available: https://nanoreview.net/en/soc-list/rating